Original Article

Effect of Bone Marrow-Derived Mesenchymal Stem Cells on the Hippocampal CA1 Area of Aluminium Chloride-Induced Alzheimer's Disease in Adult Male Albino Rat: A Histological and Immunohistochemical Study

Eman Mohammed El-Beltagi, Heba Hassan ElKaliny, Khaled Ahmed Moustafa, Gehan Mohammed Soliman and Abd-El Moniem Fareed Zamzam

Department of Histology and Cell Biology, Faculty of Medicine, Tanta University, Egypt

ABSTRACT

Introduction: Alzheimer's disease (AD) is the commonest cause of dementia among the elderly. Aluminium is a toxic metal that primarily affects the hippocampus. Bone marrow-derived mesenchymal stem cells (BM-MSCs) therapy is considered a recent strategy for treatment of several diseases including neurologic disorders.

Aim of Work: To study effect of BM-MSCs on CA1 of the experimentally induced AD in adult male albino rat.

Materials and Methods: 35 adult male albino rats were divided into a control group and an experimental group which was further subdivided into subgroups E1, E2, E3 & E4. Rats of experimental group received 17 mg/kg of aluminium chloride (AlCl3) orally once daily for 4 weeks. 24 hours after last dose of AlCl3, each rat of subgroups E2 and E3 was once IV injected with 1 ml media and BM-MSCs respectively. Subgroup E4 was the recovery subgroup. Hippocampal CA1 specimens were obtained and processed for histological, immunohistochemical, electron microscopic and morphometric studies.

Results: Subgroups E1 and E2 revealed many structural changes as disarrangement of pyramidal cell layer which exhibited deeply stained nuclei and vacuolated cytoplasm. Congo red stain of these subgroups showed Congo red positive pyramidal cells and electron microscopic examination showed swollen destroyed mitochondria and dilated saccules of Golgi stacks. Statistically, there was a highly significant increase in number of neurofibrillary tangles and a highly significant decrease in synaptophysin color intensity. In contrast, these changes were markedly ameliorated in the BM-MSCs-treated subgroup. On the other hand, the recovery subgroup showed persistence of some of the structural changes.

Conclusion: BM-MSCs injection can ameliorate AD-like pathology which was induced by AlCl3 in CA1 of adult male albino rats.

INTRODUCTION

Alzheimer's disease (AD) is one of the major medical challenges nowadays. About 30 million people worldwide are suffering from AD. The number is expected to increase to 100 million by 2050 unless effective prevention or therapy is detected[1]. AD is the most prevalent form of dementia. It is a progressive neurodegenerative disease characterized by memory impairment and cognitive dysfunction[2,3].

Old age (65 or older) and family history of AD are unmodifiable risk factors for this disease. Meanwhile, diabetes mellitus, obesity, smoking, hypertension, low educational level and lack of social engagement are considered as modifiable risk factors[4]. It has been reported that excessive amounts of β-amyloid peptide in the brain are responsible for AD-related pathology, including amyloid plaques, intracellular neurofibrillary tangles, neurite dystrophy, dendritic spine loss, synapse loss and neuronal cell death[5].

Symptoms of AD vary among individuals. The most common initial symptom is a gradually worsening ability to remember new information. This occurs because the first neurons to be damaged are usually in the hippocampus that is involved in forming new memories. Later on, neurons in other brain areas are damaged, so, the individuals experience difficulties in solving problems and completing familiar tasks, confusion with time or place, social withdrawal, depression and sleep disturbances[4].

The current therapeutic options have focused on ameliorating the symptoms as well as reducing the rate of progression[6]. They include acetylcholinesterase inhibitors, N-Methyl-D-aspartate receptor antagonists and serotonin receptor antagonists[7]. Etiology-based treatment is under clinical trials including amyloid binders and anti-β-amyloid aggregation compounds[8]. However, these treatments only provide symptomatic relief over a short period of time with many side effects and variable efficacy from patient to patient[9].

Aluminium chloride (AlCl3) is a well-known neurotoxin. The neurotoxicity induced by AlCl3 resembles the progressive neurodegenerative changes observed in AD. Therefore, AlCl3 administration has been widely used to induce AD model[10].

Recently, different stem cell therapies have been tested in both animal models and clinical trials and become a promising solution to treat many human diseases. Mesenchymal stem cells (MSCs) are group of multipotent stem cells which are widely used and offer a great promise to treat several neurologic disorders[11].

The main underlying mechanism for beneficial effects of MSCs in tissue regeneration is based on their capability to produce a variety of trophic factors which can stimulate neighboring parenchymal cells to start repairing damaged tissues. In addition, these trophic factors can modulate the local immune system, enhance angiogenesis, prevent cell apoptosis and stimulate proliferation and differentiation of resident tissue specific stem cells[12].

In the present study, choosing CA1 hippocampal area for studying the pathological findings of AD came from the fact that it is one of the earliest and most vulnerable brain regions to AD. CA1 neuronal degeneration directly underlies the cognitive dysfunction and memory loss, which are the initial symptoms of AD[13,14]. Therefore, the present work was designed to investigate the effect of BM-MSCs on CA1 hippocampal area of the experimentally induced AD in adult male albino rat.

MATERIALS AND METHODS

Animals

The present study was carried out on 35 adult male albino rats (160-200 gm each). After being grouped, the animals were housed in suitable clean properly ventilated plastic cages with mesh wire under similar good illumination conditions. They were fed on a similar commercial laboratory food and water. In addition, they were acclimatized to their environment for two weeks before starting the experiment which was approved by the local ethical committee, Faculty of Medicine, Tanta University (approval code number: 32460/07/18). All the experiments were performed at the Histology and Cell Biology Department, Faculty of Medicine, Tanta University.

Induction of AD

Aluminium chloride (AlCl3) was used to induce AD. It was obtained in the form of powder as a bottle of 500 gm of AlCl3 from El-Gomhoria Company for Trading Pharmaceutical Chemicals and Medical Appliances, Tanta, Egypt (CODE No. L04200).

Isolation and culture of BM-MSCs[15,16]

The bone marrow of femurs, tibias and humeri was flushed out from the diaphysis. The marrow plugs were cultured with freshly prepared media (RPMI, 10% FBS and 1% Antibiotic /Antimycotic mix) (RPMI from Lonza Com, Cat. No. BE12-702F, Swiss. FBS from Gibco, In*vitro*gen Com, Cat. No. A11-151, Austria. Antibiotic/Antimycotic mix from Lonza Com, Cat. No. 17-745 E, Switzerland) in tissue culture flasks that were kept at 37 °C in 5% CO2 incubator. The cultured cells were examined by the phase contrast microscope to assess level of expansion. Three days after culture, the non-adherent cells were removed. BM-MSCs were distinguished from other marrow cells by their tendency to adhere to tissue culture flask. When BM-MSCs reached confluence (70-80%), trypsinization and subculturing was done by applying 2.5 ml of trypsin/EDTA solution. The hemocytometer was used to determine the total cell count and the trypan blue 0.4% exclusion method was used to assess cells viability. The cells were injected at a dose of 3×10^6/rat[17]. All cell culture procedures were done at the Tissue Culture Unit, Histology and Cell Biology Department, Faculty of Medicine, Tanta University.

Experimental design

The rats were divided into two main groups:

I- Control group (C): was subdivided into 3 subgroups, 5 rats for each:

- **Subgroup C1:** was kept without treatment. Control hippocampus specimens were obtained. In addition, bone marrow of animals was collected.

- **Subgroup C2:** received 0.85 ml distilled water /100 gm orally via gastric tube once daily for 4 weeks, after which hippocampus specimens were obtained.

- **Subgroup C3:** received a single IV injection in the tail vein with 1 ml media used for suspension of BM-MSCs. Hippocampus specimens were obtained after 4 weeks from media injection.

II- Experimental group (E): was subdivided into 4 subgroups, 5 rats for each:

- **Subgroup E1** (AlCl3-treated subgroup): received AlCl3 at a dose of 17 mg/kg orally by a gastric tube once daily for 4 weeks[18]. The calculated dose was obtained by dissolving 200 mg of AlCl3 in 100 ml distilled water. Each rat was given 0.85 ml/100 gm of this prepared solution. Hippocampus specimens were obtained 24 hours after the last dose of AlCl3.

- **Subgroup E2** (Media-treated subgroup): received AlCl3 as subgroup E1, then each rat was once intravenously injected with 1 ml media, 24 hours after the last dose of AlCl3. Hippocampus specimens were obtained after 4 weeks from media injection.

- **Subgroup E3** (BM-MSCs-treated subgroup): received AlCl3 as subgroup E1, then each rat received BM-MSCs (3×10^6) suspended in its specific media, 24 hours after the last dose of AlCl3 by single IV injection in the tail vein. Hippocampus specimens were obtained after 4 weeks from BM-MSCs injection[17].

- **Subgroup E4** (Recovery subgroup): received AlCl3 as subgroup E1. Rats were kept without any treatment for another 4 weeks, after which hippocampus specimens were obtained.

Histological studies

At the appropriate time, the animals were anesthetized by an intraperitoneal injection of sodium thiopental (30 mg/kg)[19]. The hippocampi were dissected and specimens were processed for histological, immunohistochemical and electron microscopic studies that were performed at the Histology and Cell Biology Department, Faculty of Medicine, Tanta and Al-Azhar Universities.

I- Light microscopic studies

Specimens were immediately fixed in formaldehyde for 24 hours, dehydrated, cleared, impregnated in a pure soft paraffin and then embedded in hard paraffin. Serial coronal sections were cut at 5-µm thickness by a rotary micro¬tome (Leitz, 1512, Germany)[20]. The sections were stained by the following methods:

1. Haematoxylin and eosin (H&E) stains[21].

2. Congo red stain for detection of amyloid granules[22].

3. Silver stain for detection of neurofibrillary tangles[23].

4. Immunohistochemical staining for detection of synaptophysin protein[24]:

Sections were deparaffinized, rehydrated and incubated in hydrogen peroxide (10%) for 10-15 minutes. The sections were immersed in a citrate buffer solution (PH 6) in a microwave for 10-20 minutes for antigen retrieval. Sections were left to cool for 20 minutes at room temperature. Slides were washed for 2 times in buffer (0.05% sodium azide). Monoclonal mouse anti-synaptophysin primary antibody (Sigma Aldrich, Egypt) was applied. Slides were washed for 4 times in buffer. Biotinylated secondary goat-anti mouse antibody (Nova Castra Laboratories Ltd, UK) was applied. Slides were incubated for 10 minutes at room temperature and then washed in buffer. Diaminobenzidine (DAB) was applied as a chromogen. Mayer's haematoxylin was used as a counter stain. The synaptophysin positive sites of reaction at the nerve cells surface and in the neuropil were stained brown and the nuclei were stained blue. In negative control slides, the same method was applied with replacement of monoclonal antibody by diluted bovine serum. Whole brain specimens were used as positive control.

II- Electron microscopic study[25,26]

Specimens were fixed in 2.5% phosphate buffered glutaraldehyde and processed by routine protocol. Semithin sections (1 µm thick) were obtained, stained with toluidine blue and examined. Ultrathin sections (75 nm) were stained with uranyl acetate and lead citrate to be examined by JEOL electron microscope at the Electron Microscopic Units of Tanta and Mansoura Universities.

Morphometric study

Olympus light microscope was used for imaging at Histology and Cell Biology Department, Faculty of Medicine, Tanta University. The software (Image J) program (National Institute of Health, Bethesda, Maryland, USA) was used. The number of neurofibrillary tangles and the color intensity of synaptophysin immunoreactivity were counted in 5 non-overlapping fields from each slide of each rat of each group at a magnification of 400.

Statistical analysis

The data were analyzed by performing one way analysis of variance (ANOVA) test followed by Tukey's test to compare different subgroups using statistical package for social sciences (version 11.5; SPSS IBM Incorp., New York, USA). All values were expressed as mean ± standard deviation (SD). Results were regarded as statistically significant if probability value (P) <0.05 and highly significant if P <0.001[27].

RESULTS

I- Morphological characterization of BM-MSCs

The adherent BM-MSCs showed multiple interdigitating processes and central nuclei with multiple nucleoli (Figure 1).

II- Light microscopic results

1- H&E stained sections

Sections obtained from the hippocampi of all subgroups of the control animals revealed the same normal histological structure. The hippocampus appeared as a pair of interlocking C-shaped structures; the cornu ammonis (CA) and the dentate gyrus. The CA was arranged as CA1, CA2, CA3 and CA4 areas (Figure 2A). CA1 area was arranged into outer polymorphic, middle pyramidal and inner molecular layers. The pyramidal cell layer contained closely packed pyramidal neurons arranged in 2-3 rows. These cells exhibited large rounded vesicular nuclei with prominent nucleoli surrounded by scanty basophilic cytoplasm and apical dendrites that extended into the molecular layer. Both the polymorphic and molecular layers contained small blood vessels and neuroglial cells with small nuclei. They were scattered among an eosinophilic background of the neuropil which consisted of neuronal and neuroglial cell processes (Figure 2B).

Examination of sections obtained from subgroup E1 (AlCl3-treated) revealed disturbance in CA1 architecture. The disarranged pyramidal cell layer illustrated displacement of many pyramidal cells mainly into the polymorphic layer and some into the molecular layer (Figure 3A). Other sections revealed an apparent reduction in the pyramidal cell layer thickness (Figure 3B). Some pyramidal cells appeared with shrunken deeply stained pyknotic nuclei, while others showed

fragmented karyorrhexitic nuclei in addition to crescent shaped nuclei with chromatin margination. The cytoplasm of some cells was vacuolated and acidophilic. Furthermore, some pyramidal cells exhibited corkscrew dendrites. Some neuroglial cells exhibited darkly stained nuclei within the vacuolated neuropil. Other neuroglia appeared fused together. Moreover, some areas in the neuropil revealed focal hemorrhage (Figures 3A,B,C). Sections obtained from subgroup E2 (Media-treated) revealed similar structural changes as the previous subgroup (Figure 3D).

In contrast, sections obtained from subgroup E3 (BM-MSCs-treated) showed more or less normal histological structure of CA1 area. Few pyramidal cells exhibited deeply stained nuclei (Figure 4). On the other hand, subgroup E4 (Recovery subgroup) showed persistent some structural changes like vacuolated pyramidal neurons with shrunken deeply stained nuclei. The neuroglial cells illustrated deeply stained nuclei and surrounded by vacuolated neuropil (Figure 5).

2- Congo red stained sections

Examination of sections obtained from the control animals revealed no Congo red positive pyramidal neurons in CA1 area (Figure 6A). Sections obtained from the AlCl3-treated and the media-treated subgroups (E1&E2) showed many Congo red positive pyramidal cells (Figures 6B,C). On the other hand, sections obtained from the BM-MSCs-treated subgroup (E3) showed few localized areas with few Congo red positive pyramidal cells (Figure 6D). Recovery subgroup (E4) depicted the same findings like subgroups E1&E2 (Figure 6E).

3- Silver stained sections

Examination of sections from the control animals revealed no intracellular neurofibrillary tangles in the pyramidal cells of CA1 area (Figure 7A). Sections from the AlCl3-treated and the media-treated subgroups showed many pyramidal cells with intracellular neurofibrillary tangles (Figures 7B,C). The BM-MSCs-treated subgroup (E3) showed absence of intracellular neurofibrillary tangles in most of the examined fields. However, few areas illustrated few pyramidal cells with intracellular neurofibrillary tangles (Figure 7D). Meanwhile, the recovery subgroup showed some pyramidal cells with intracellular neurofibrillary tangles (Figure 7E).

4- Synaptophysin immunostaining

Immunostained sections obtained from the control animals exhibited an apparent strong synaptophysin positive reaction in the form of fine beaded reactivity at the pyramidal cells surface and in the neuropil (Figure 8A). Sections from the AlCl3-treated and the media-treated subgroups (E1&E2) showed an apparent weak synaptophysin positive reaction at the same corresponding areas (Figures 8B,C). The BM-MSCs-treated subgroup (E3) showed an apparent strong synaptophysin positive reaction at the equivalent related regions (Figure 8D). Whereas, the recovery subgroup (E4) showed an apparent weak synaptophysin positive reaction (Figure 8E).

Morphometric and Statistical results

The mean number of neurofibrillary tangles illustrated a non-significant difference in subgroup E3 as compared with the control group. Subgroups E1, E2 and E4 showed a highly significant increase as compared with the control group (Table 1, Histogram 1).

The mean color intensity of synaptophysin immunoreaction illustrated a non-significant difference in subgroup E3 as compared with the control group. Subgroups E1, E2 and E4 showed a highly significant decrease as compared with the control group (Table 1, Histogram 2).

III- Electron microscopic results

Electron microscopic examination of the ultrathin sections of the CA1 area obtained from the control animals revealed its normal electron microscopic picture. The pyramidal cells contained large euchromatic nuclei surrounded by abundant polyribosomes, rough endoplasmic reticulum (RER), multiple perinuclear Golgi stacks, mitochondria and few lysosomes (Figure 9A). The polymorphic and molecular layers contained their cellular processes in addition to neuroglial cells and blood capillaries among the neuropil. The myelin sheath of the myelinated nerve fibers appeared thick, electron dense, continuous and tightly wrapped around the axon (Figure 9B). The oligodendrocytes had indented nuclei, RER and mitochondria (Figure 9C). The astrocytes contained oval to rounded euchromatic nuclei, mitochondria and polyribosomes (Figure 9D). The blood capillaries were lined by a single layer of continuous endothelial cells resting on a continuous basement membrane. Some astrocytes and pericytes appeared beside these blood capillaries (Figure 9E).

Sections of subgroup E1 (AlCl3-treated) revealed prominent ultrastructural changes. The pyramidal cells showed apparent small nuclei with areas of clumped chromatin, destroyed mitochondria, dilated unstacked saccules of Golgi apparatus, vacuoles and many lysosomes (Figure 10A). The myelin sheath of the myelinated nerve fibers exhibited splitting of its layers (Figure 10B). The oligodendrocytes revealed irregular nuclei with dilated perinuclear cisternae, dilated RER, swollen mitochondria with partial loss of cristae and dilated disorganized saccules of Golgi stack (Figure 10C). As regards the blood capillaries, the nuclei of the lining endothelial cells illustrated dilated perinuclear cisternae and a focally disrupted nuclear membrane. In addition, the basement membrane was disrupted and the perivascular astrocytic foot processes were vacuolated (Figure 10D). Some areas in the neuropil exhibited an apparent microgliosis, where some microglial cells revealed elongated or irregular nuclei and many lysosomes (Figure 10E).

Sections obtained from subgroup E2 (Media-treated) revealed similar results as the previous subgroup (Figures 11A,B,C,D).

On the other hand, the BM-MSCs-treated subgroup (E3) revealed preservation of ultrastructural integrity of CA1. The pyramidal cells appeared more or less normal (Figure 12A). In addition, the myelin sheath of the myelinated nerve fibers appeared more or less normal (Figure 12B). The neuropil revealed more or less normal oligodendrocytes except some cells with fragmented chromatin, more or less normal astrocytes and blood capillaries (Figures 12C,D,E).

However, the recovery subgroup (E4) revealed maintenance of some ultrastructural alterations in CA1

like pyramidal cells with dilated perinuclear cisternae, swollen mitochondria with destroyed cristae, lysosomes, autophagosomes and dissociated unstacked Golgi apparatus (Figure 13A). The myelin sheath of some myelinated nerve fibers showed splitting of its layers (Figure 13B). The nearby neuroglia demonstrated cytoplasmic vacuoles and dilated saccules of Golgi stack mainly in oligodendrocytes (Figure 13C) and astrocytes (Figure 13D). Some blood capillaries illustrated dilated perinuclear cisternae of the lining endothelial cells and vacuolated perivascular astrocytic foot processes (Figure 13E).
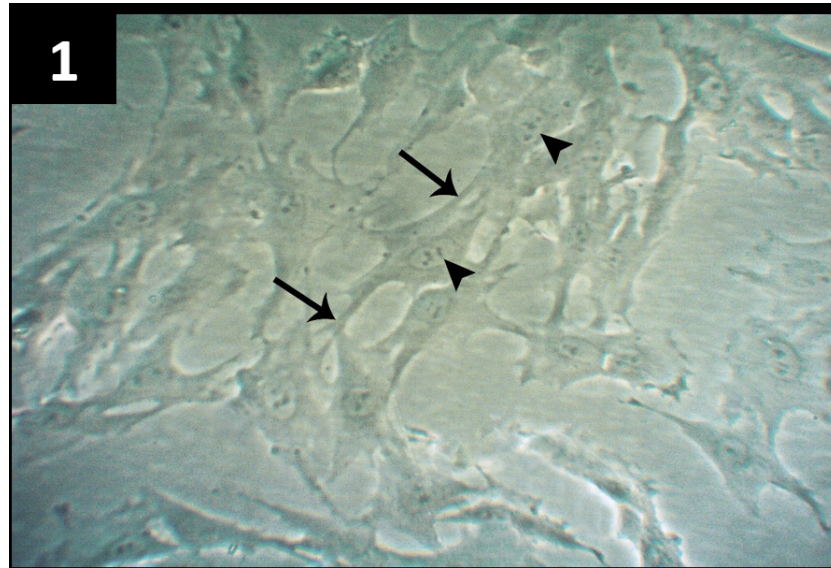

Fig. 1: A photomicrograph of rat BM-MSCs. The cultured cells have multiple interdigitating processes (arrows) and central vesicular nuclei with prominent nucleoli (arrow heads). (Phase contrast microscope x 400).
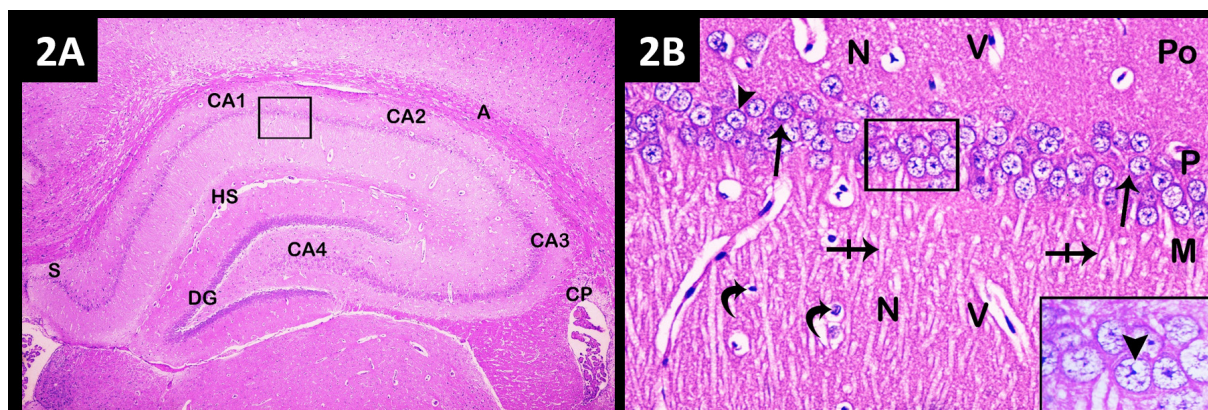

Fig. 2: A photomicrograph of a control rat hippocampus. (A) The CA appears arranged into CA1, CA2, CA3 & CA4 areas. The dentate gyrus (DG), subiculum (S), alveus (A), choroid plexus (CP) and hippocampal sulcus (HS) can be seen. (H&E x 40). (B) CA1 area appears arranged into polymorphic (Po), pyramidal (P) and molecular (M) layers. The pyramidal layer contains 2-3 rows of closely packed pyramidal cells having rounded vesicular nuclei with prominent nucleoli (arrow heads), scanty basophilic cytoplasm (arrows) and apical dendrites (crossed arrows) extending into the molecular layer. Neuroglial cells (curved arrows) and small blood vessels (V) are scattered among an eosinophilic background of the neuropil (N). (H&E x 400, Inset x 1000).
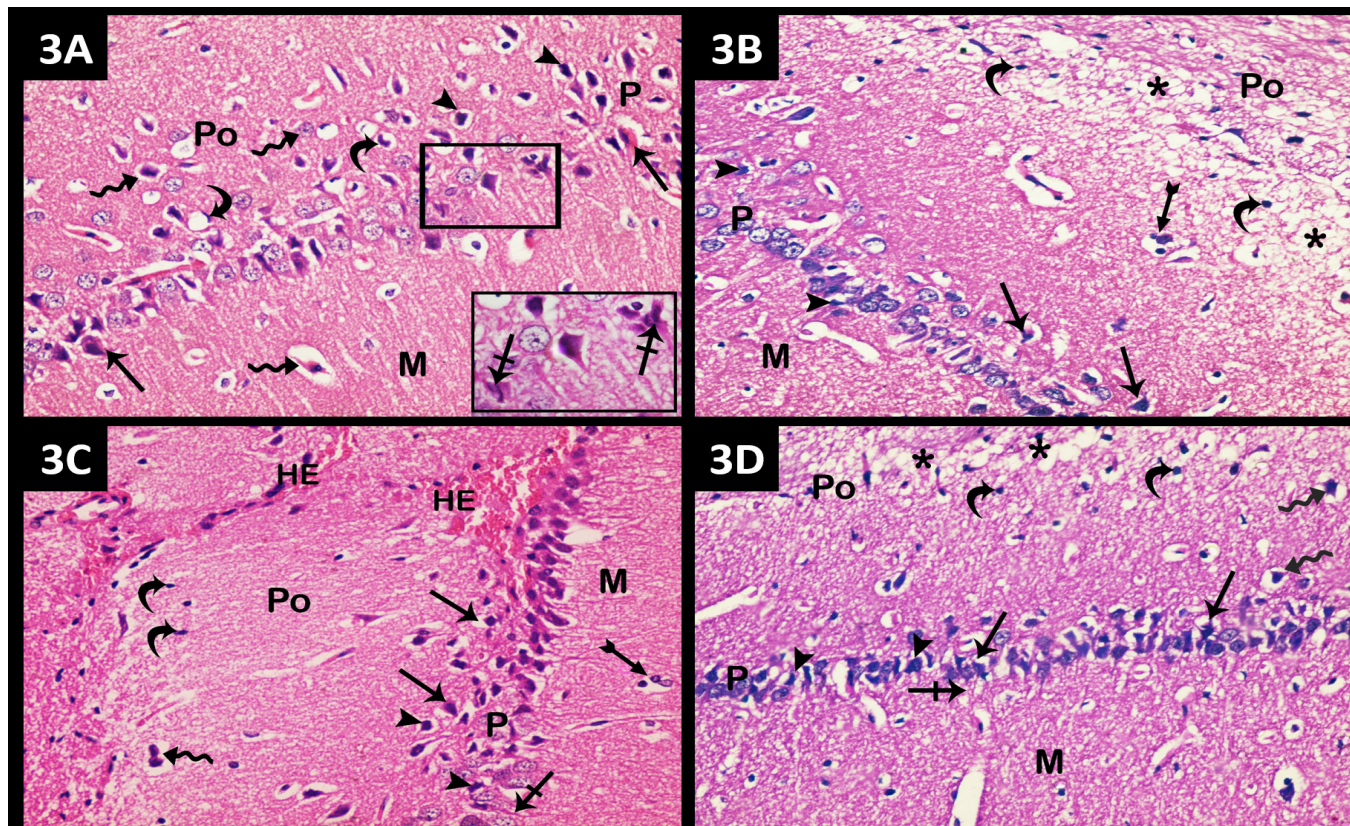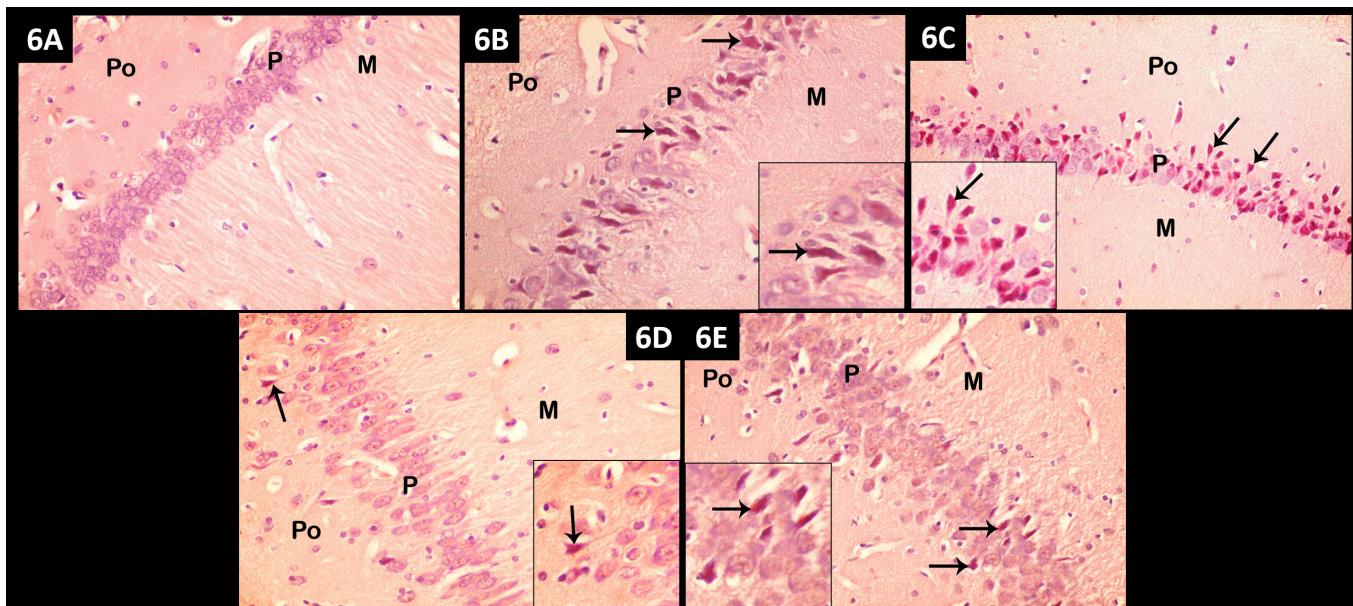
Fig. 3: A photomicrograph of a rat CA1: (A) Subgroup E1 showing disarranged pyramidal cell layer (P) with displacement of many pyramidal cells (wavy arrows) mainly into the polymorphic layer (Po) and some into the molecular layer (M). Some pyramidal cells show shrunken deeply stained pyknotic nuclei (arrow heads), fragmented karyorrhexitic nuclei (crossed arrows) and crescent shaped nuclei (curved arrows). The cytoplasm of some cells is vacuolated and acidophilic (arrows). (H&E x 400, Inset x 1000). (B) Subgroup E1 showing an apparent reduction in the pyramidal cell layer thickness (P). Some pyramidal cells show deeply stained nuclei (arrow heads) and vacuolated acidophilic cytoplasm (arrows). Some neuroglial cells exhibit darkly stained nuclei (curved arrows). Some of them are fused together (tailed arrow). The neuropil of the polymorphic layer (Po) shows vacuolation (*). M; molecular layer. (H&E x 400). (C) Subgroup E1 showing focal hemorrhage (HE). Some neuroglia with darkly stained nuclei (curved arrows) are observed. Other neuroglia are fused together (tailed arrow). Many pyramidal cells illustrate deeply stained nuclei (arrow heads), vacuolated acidophilic cytoplasm (arrows) and corkscrew dendrites (crossed arrow). Some displaced nerve cells with deeply stained nuclei are fused together (wavy arrow). Po; polymorphic, P; pyramidal and M; molecular layers. (H&E x 400). (D) Subgroup E2 showing an apparent reduction in pyramidal cell layer thickness (P). The pyramidal cells show deeply stained nuclei (arrow heads), vacuolated cytoplasm (arrows) and corkscrew dendrites (crossed arrow). Some of them appear displaced (wavy arrows) into the polymorphic layer (Po). The neuroglia exhibit deeply stained nuclei (curved arrows) and the neuropil shows vacuolation (*). M; molecular layer. (H&E x 400).
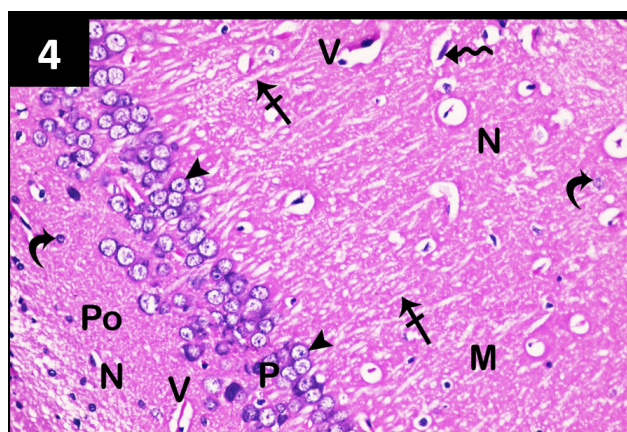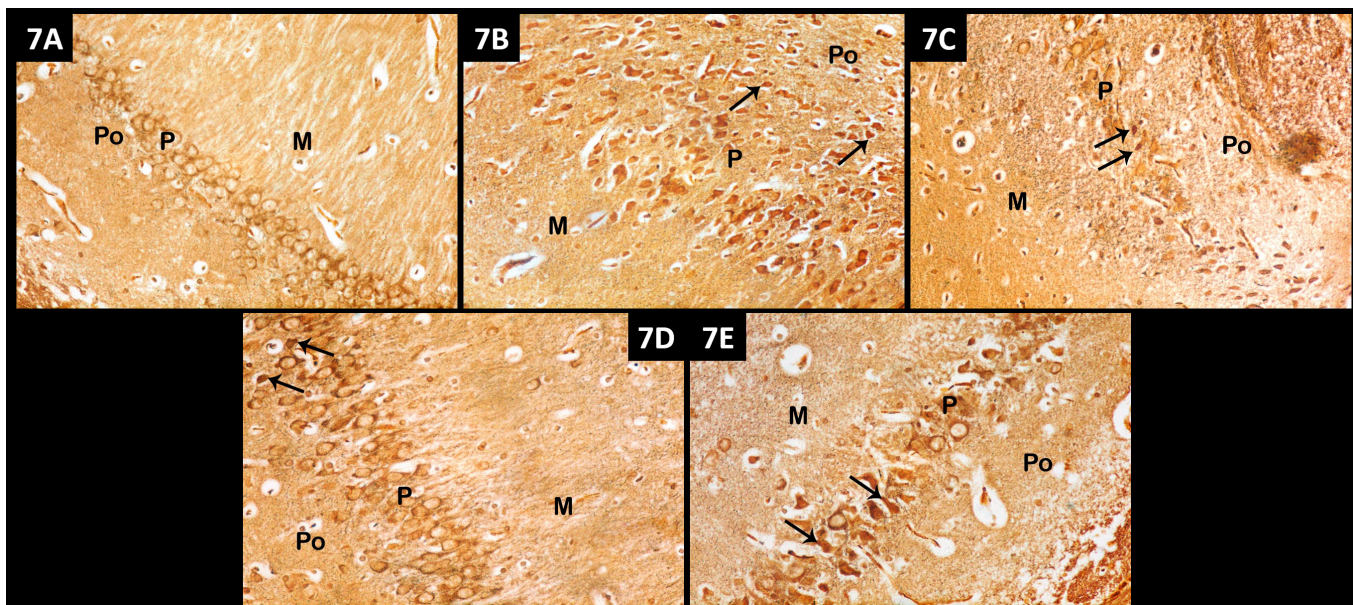

Fig. 4: A photomicrograph of a rat CA1 of subgroup E3 showing well-arranged polymorphic (Po), pyramidal (P) and molecular (M) layers. The pyramidal cells are regularly arranged in compact rows, having rounded vesicular nuclei with prominent nucleoli (arrow heads) and apical dendrites (crossed arrows). Neuroglia (curved arrows) and small blood vessels (V) are scattered among the neuropil (N). A nerve cell with a deeply stained nucleus (wavy arrow) appears displaced into the molecular layer. (H&E x 400).
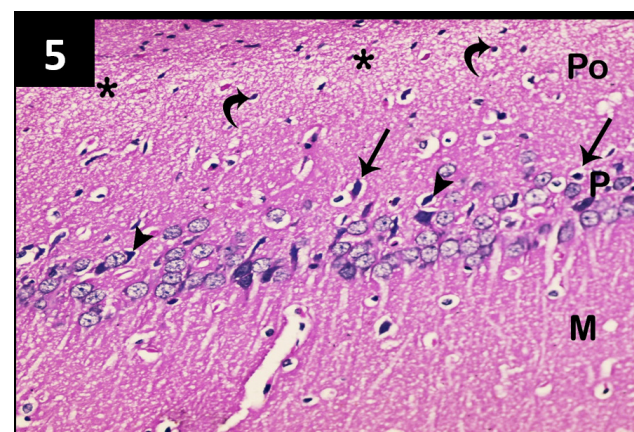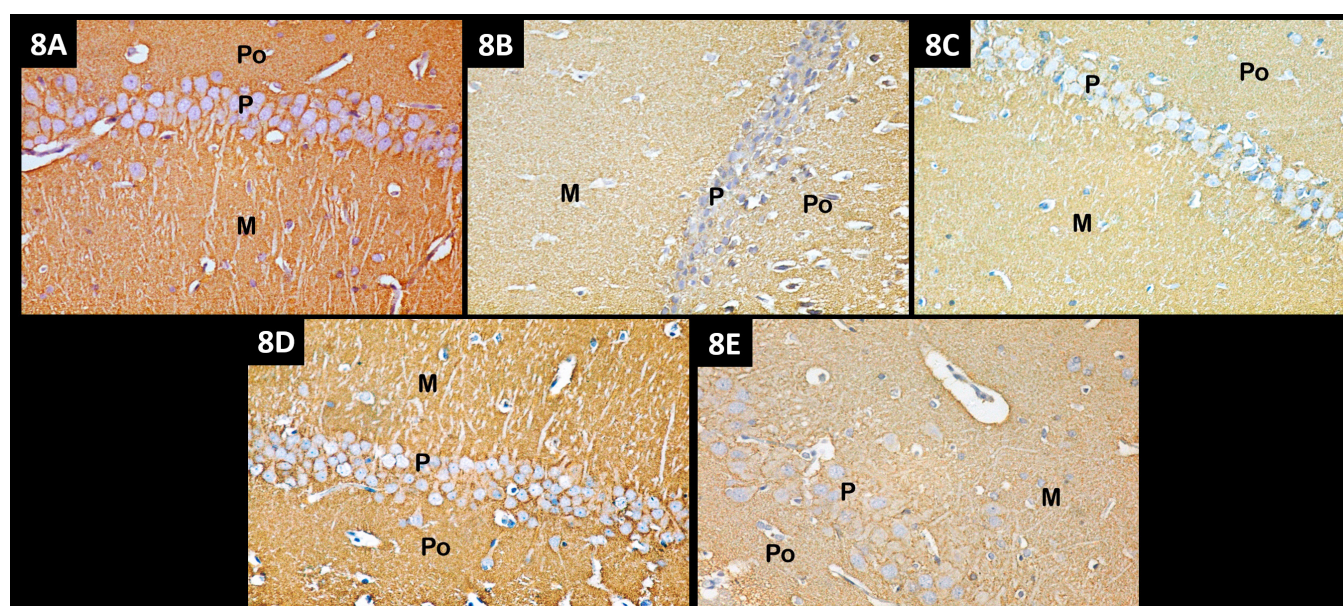

Fig. 5: A photomicrograph of a rat CA1 of subgroup E4 showing the polymorphic (Po), pyramidal (P) and molecular (M) layers. Some pyramidal cells show shrunken deeply stained nuclei (arrow heads) and vacuolated cytoplasm (arrows). The neuroglial cells illustrate deeply stained nuclei (curved arrows) and the neuropil is vacuolated (*). (H&E x 400).

Fig. 6: A photomicrograph of Congo red stained sections of a rat CA1: (A) Control group showing no Congo red positive pyramidal cells. (B) Subgroup E1 depicts many Congo red positive pyramidal cells (arrows). (C) Subgroup E2 viewing many Congo red positive pyramidal cells (arrows). (D) Subgroup E3 demonstrates few Congo red positive pyramidal cells (arrows). (E) Subgroup E4 showing some Congo red positive pyramidal cells (arrows). M; molecular, P; pyramidal and Po; polymorphic layers. (Congo red x 400).

Fig. 7: A photomicrograph of silver stained sections of a rat CA1: (A) Control group showing no intracellular neurofibrillary tangles within the pyramidal cells. (B) Subgroup E1 showing many pyramidal cells with intracellular neurofibrillary tangles (arrows). (C) Subgroup E2 showing many pyramidal cells with intracellular neurofibrillary tangles (arrows). (D) Subgroup E3 showing few pyramidal cells with neurofibrillary tangles (arrows). (E) Subgroup E4 showing some pyramidal cells with neurofibrillary tangles (arrows). M; molecular, P; pyramidal and Po; polymorphic layers. (Silver x 400).

Fig. 8: A photomicrograph of immuno-stained sections of a rat CA1: (A) Control group showing an apparent strong synaptophysin positive immunoreaction at the pyramidal cells surface and in the neuropil. (B) Subgroup E1 showing an apparent weak synaptophysin positive immunoreaction. (C) Subgroup E2 showing an apparent weak synaptophysin positive immunoreaction. (D) Subgroup E3 showing an apparent strong synaptophysin positive immunoreaction. (E) Subgroup E4 showing an apparent weak synaptophysin positive immunoreaction. M; molecular, P; pyramidal and Po; polymorphic layers. (Synaptophysin immunostaining & H x 400).
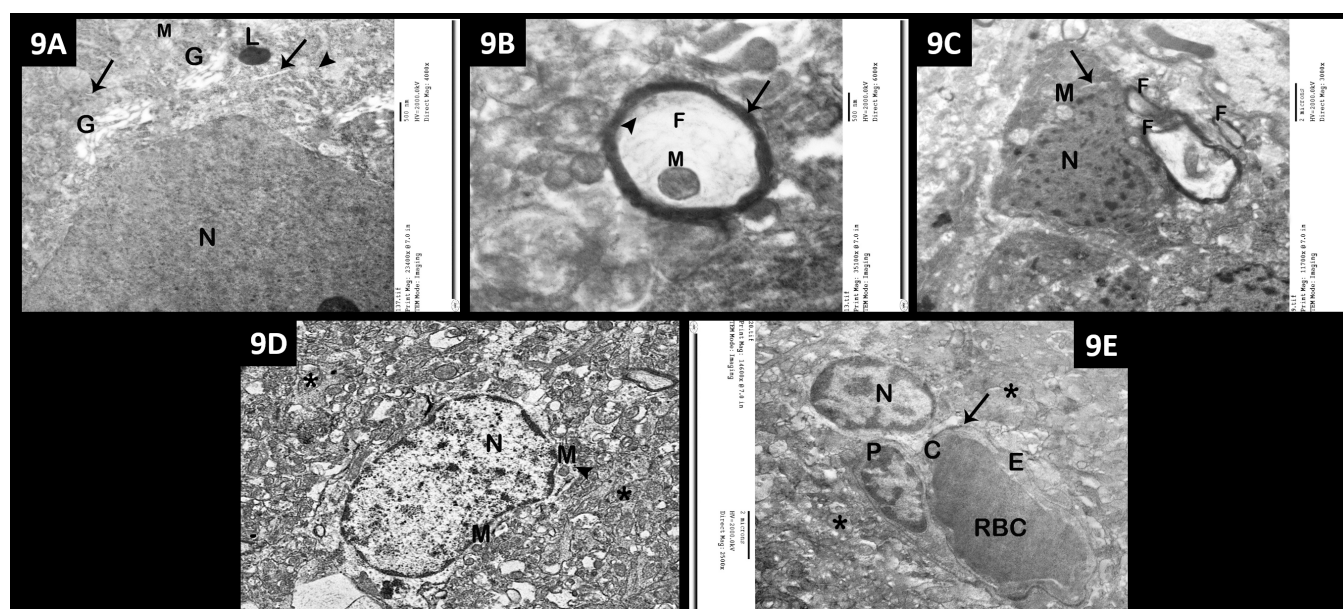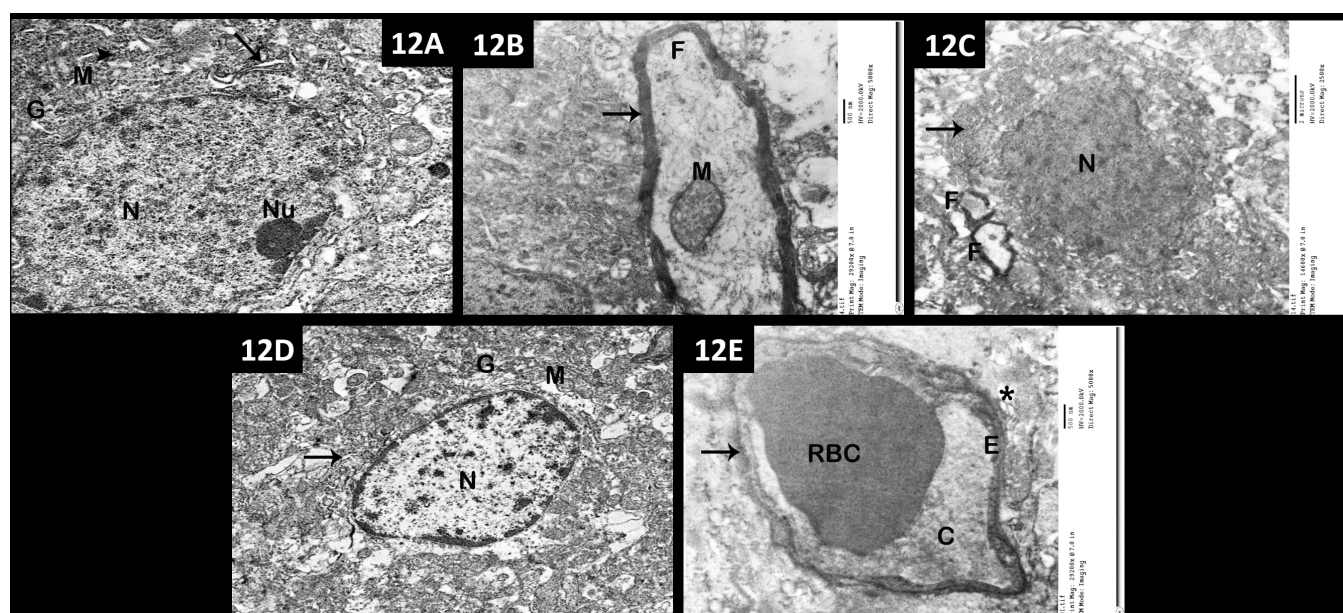

Fig. 9: An electron micrograph of a control rat CA1: (A) A pyramidal cell having a large euchromatic nucleus (N) surrounded by abundant polyribosomes (arrow head), RER (arrows), multiple perinuclear Golgi stacks (G), mitochondria (M) and few lysosomes (L). (x 4000). (B) A myelinated nerve fiber (F) containing mitochondria (M) and vesicles (arrow head) within the axoplasm. The myelin sheath appears thick, electron dense, continuous and tightly wrapped around the axon (arrow). (x 6000). (C) An oligodendrocyte containing an indented nucleus (N), RER (arrow) and mitochondria (M). Some myelinated nerve fibers (F) are seen beside the oligodendrocyte. (x 3000). (D) An astrocyte having an oval to rounded euchromatic nucleus (N), mitochondria (M) and polyribosomes (arrow head) with normal neuropil around (*). (x 3000). (E) A continuous blood capillary (C) appears lined by a single layer of continuous endothelial cells (E) resting on a continuous basement membrane (arrow). An astrocyte associated with the blood capillary appears with oval to rounded nucleus (N). Notice the nearby pericyte (P), the red blood cell (RBC) inside the lumen of the capillary and the normal neuropil (*). (x 2500).
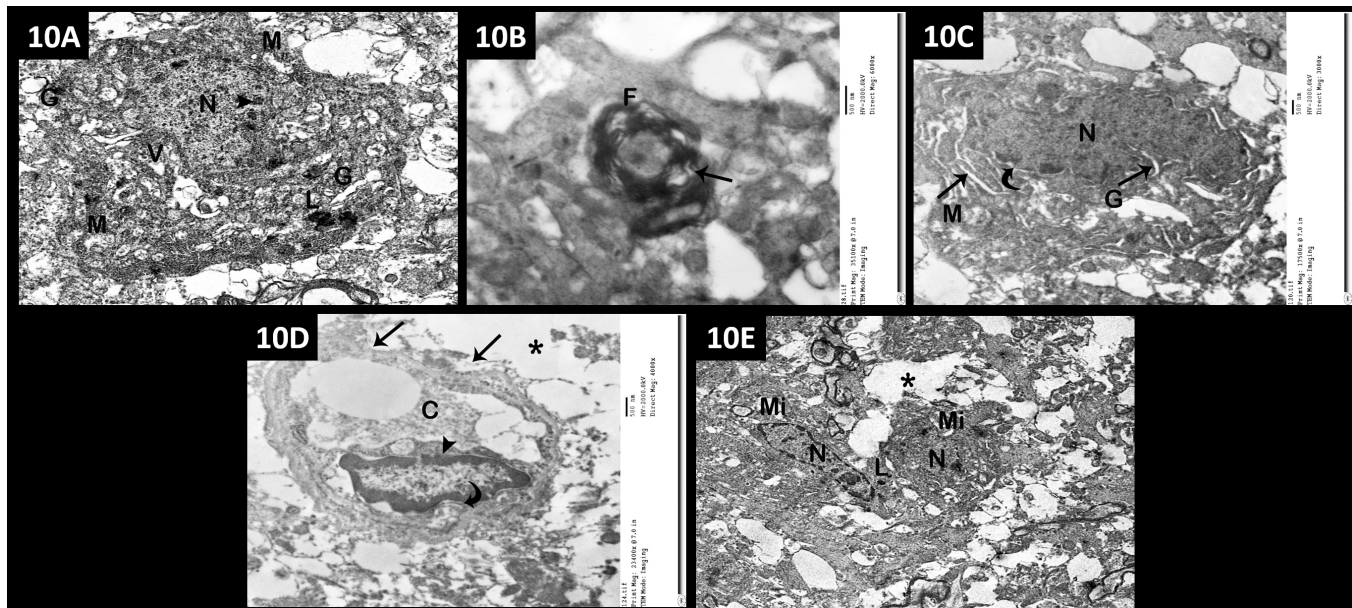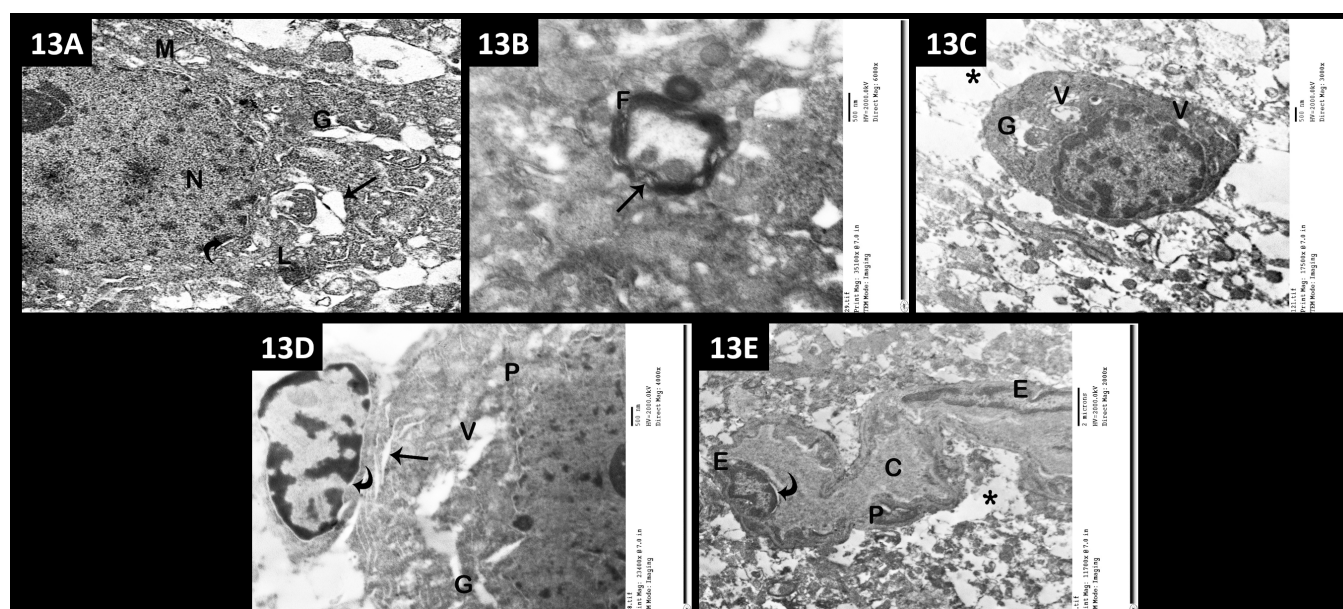
Fig. 10: An electron micrograph of a rat CA1 of subgroup E1: (A) A pyramidal cell having an apparent small nucleus (N) with areas of clumped chromatin (arrow head), dilated unstacked saccules of Golgi apparatus (G), many lysosomes (L), destroyed mitochondria (M) and vacuoles (V). (x 4000). (B) A myelinated nerve fiber (F) showing splitting of the myelin sheath layers (arrow). (x 6000). (C) An oligodendrocyte exhibiting an irregular nucleus (N) with dilated perinuclear cisterna (curved arrow), dilated RER (arrows), swollen mitochondria with partial loss of cristae (M) and dilated disorganized saccules of Golgi stack (G). (x 3000). (D) A blood capillary (C) showing a disrupted basement membrane (arrows). The lining endothelial cell has dilated perinuclear cisterna (curved arrow) and a focally disrupted nuclear membrane (arrow head). The perivascular astrocytic foot processes are vacuolated (*). (x 4000). (E) An apparent microgliosis (Mi) within the vacuolated neuropil (*). The microglial cells appear with elongated or irregular nuclei (N) and many lysosomes (L). (x 2500).
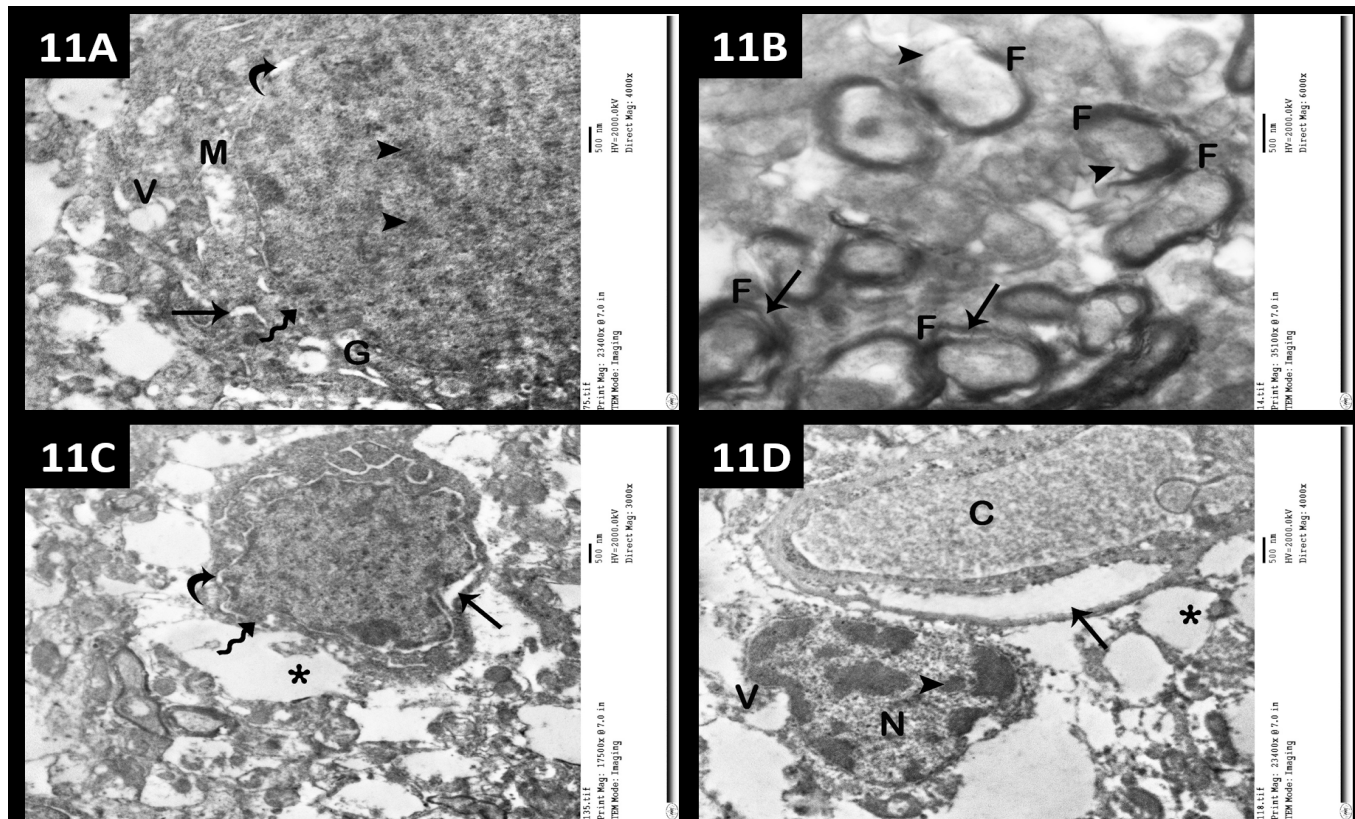
Fig. 11: An electron micrograph of a rat CA1 of subgroup E2: (A) A pyramidal cell showing dilated perinuclear cisterna (curved arrow), disrupted nuclear membrane (wavy arrow), some areas of clumped heterochromatin (arrow heads), dilated RER (arrow), dilated saccules of Golgi stack (G), vacuoles (V) and swollen mitochondria (M). (x 4000). (B) A myelinated nerve fiber (F) showing splitting (arrows) and discontinuity (arrow heads) of the myelin sheath layers. (x 6000). (C) An oligodendrocyte illustrating a focally disrupted nuclear membrane (wavy arrow), dilated perinuclear cisterna (curved arrow), dilated RER (arrow) and pericellular vacuolations (*). (x 3000). (D) A blood capillary (C) exhibiting splitting of the basement membrane (arrow). An associated astrocyte has an irregular nucleus (N) with areas of clumped chromatin (arrow head) and vacuolated cytoplasm (V). The perivascular astrocytic foot processes are vacuolated (*). (x 4000).

Fig. 12: An electron micrograph of a rat CA1 of subgroup E3: (A) A pyramidal cell containing a large euchromatic nucleus (N) with a prominent nucleolus (Nu), abundant polyribosomes (arrow head), RER (arrow) and mitochondria (M). (x 4000). (B) A myelinated nerve fiber (F) containing mitochondria (M) within the axoplasm. The myelin sheath appears thick, electron dense, continuous and tightly wrapped around the axon (arrow). (x 5000). (C) An oligodendrocyte containing a nucleus (N) with some areas of fragmented chromatin and more or less normal RER (arrow). Some myelinated nerve fibers (F) can be seen beside the oligodendrocyte. (x 2500). (D) An astrocyte having more or less normal rounded to oval euchromatic nucleus (N), mitochondria (M), RER (arrow) and saccules of Golgi stack (G). (x 3000). (E) A more or less normal blood capillary (C) appears lined by a single layer of continuous endothelial cells (E) resting on continuous basement membrane (arrow) and surrounded by astrocytic foot processes (*). Note: a red blood cell (RBC) can be seen inside the lumen of the capillary. (x 5000).

Fig. 13: An electron micrograph of a rat CA1 of subgroup E4: (A) A pyramidal cell having a nucleus (N) with dilated perinuclear cisterna (curved arrow). The cytoplasm shows swollen mitochondria with destroyed cristae (M), autophagosome (arrow), dissociated unstacked Golgi apparatus (G) and lysosomes (L). (x 4000). (B) A myelinated nerve fiber (F) showing splitting of the myelin sheath layers (arrow). (x 6000). (C) An oligodendrocyte exhibiting cytoplasmic vacuoles (V) and dilated saccules of Golgi stack (G). The surrounding neuropil is vacuolated (*). (x 3000). (D) An astrocyte showing dilated perinuclear cisterna (curved arrow). An adjacent pyramidal nerve cell (P) showing dilated RER (arrow), dilated saccule of Golgi stack (G) and cytoplasmic vacuoles (V) can be seen (x 4000). (E) A blood capillary (C) showing dilated perinuclear cisterna (curved arrow) of one of the lining endothelial cells (E). The perivascular astrocytic foot processes are vacuolated (*). P; pericyte. (x 2000).

Table 1: Statistical analysis of number of neurofibrillary tangles and color intensity of synaptophysin in CA1 in different studied groups. Data are expressed as mean ± SD.

Groups / Parameters	Mean number of neurofibrillary tangles ± SD	Mean color intensity of synaptophysin ± SD
Control group	0±0.000	103.7238± 2.746
E1 (AlCl3-treated subgroup)	42.6±1.949*	62.406±5.715*
E2 (Media-treated subgroup)	41±2.345*	62.3628±5.622*
E3 (BM-MSCs-treated subgroup)	3.4±0.547	103.0152±2.765
E4 (Recovery subgroup)	3.564±32.2*	64.947±5.347*

P-value>0.05: non-significant, P-value<0.05: significant and P-value<0.001(*): highly significant

Number of neurofibrillary tangles in CA1
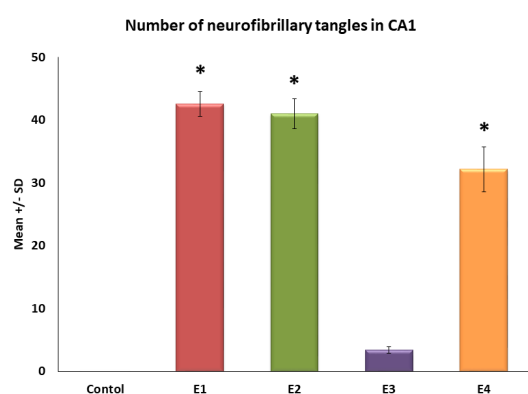
Histogram 1: The mean number of neurofibrillary tangles in CA1 area in different studied subgroups

Synaptophysin color intensity in CA1
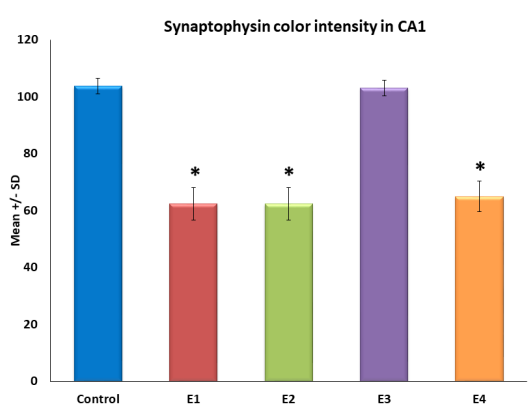
Histogram 2: The mean color intensity of synaptophysin immunoreaction in CA1 area in different studied subgroups

DISCUSSION

Alzheimer's disease (AD) is a neurodegenerative disorder which commonly affects the aged individuals. Although the Food and Drug Administration (FDA) approved some drugs for treatment of AD, there is no curative therapy until now. Beside their side effects, these drugs can only improve the daily cognitive functions to a very limited degree[28,29].

Aluminium chloride (AlCl3) is a neurotoxic metal. Mouse models of AlCl3 induced AD-like pathology have been effectively used in various studies. This is because AlCl3 can be easily administered orally and has high bioavailability[30].

The present study revealed that AlCl3 administration has a deleterious effect on the structure of CA1 of hippocampus of subgroup E1. This was in the form of disarranged pyramidal cell layer with displacement of many cells into the polymorphic and molecular layers and an apparent reduction in pyramidal cell layer thickness. Some pyramidal cells revealed pyknotic, fragmented and crescent shaped nuclei, vacuolated acidophilic cytoplasm and corkscrew dendrites.

Al-Otaibi *et al.*, (2018)[31] reported that AlCl3 administration is associated with oxidative stress and generation of reactive oxygen species (ROS). They added that the brain tissues are highly susceptible to the damaging effects of ROS due to their high rate of oxygen consumption, presence of abundant polyunsaturated fatty acids in the cell and organelles' membranes and low anti-oxidant enzymes.

Additionally, AlCl3 can induce lipid peroxidation by interacting with plasma membrane lipids. This occurs indirectly as AlCl3 binds to the iron-carrying protein transferrin, so it reduces binding of iron with an increase in the intracellular free iron level and stabilization of iron in its ferrous state that promotes ferrous-induced lipid peroxidation[32]. Previous researchers reported that peroxidation of membrane lipids can result in an increase in membrane leakiness, mitochondrial dysfunction, damage to DNA, lipids and proteins, resulting in cell degeneration and eventual cell death[33].

In the present work, subgroup E1 revealed displacement of many pyramidal cells into the polymorphic and molecular layers. This was in accordance with Zaher *et al.*, (2019)[34]. The displaced pyramidal cells were referred as ectopic neurons[35]. This displacement could be attributed to the delayed migration and settlement of these pyramidal cells into the pyramidal cell layer as a result of altered neuronal-neuroglial interaction subsequent to AlCl3 exposure. The displacement of these pyramidal cells led to disarrangement and apparent reduction of the pyramidal cell layer thickness[36].

Some pyramidal cells showed deeply stained and fragmented nuclei with areas of clumped chromatin. According to Kumar *et al.*, (2018)[37], these nuclear changes are related to cell necrosis. The nuclear shrinkage with increased basophilia is termed as pyknosis. These nuclei undergo further fragmentation which is called karyorrhexis.

In addition, some neurons exhibited crescent shaped nuclei. Previous researchers attributed the chromatin margination, nuclear pyknosis and fragmentation to be feature of cell apoptosis[38-40]. AlCl3 can induce

mitochondrial cytochrome C discharge with activation of caspases, upregulation of pro-apoptotic B cell lymphoma-2 (Bcl-2)-associated x (Bax) protein and downregulation of anti-apoptotic B cell lymphoma-2 (Bcl-2) protein, ending by mitochondria-dependent intrinsic apoptotic cell death[41].

As regards the acidophilic cytoplasm of some pyramidal cells, Haider *et al*., (2020)[42] attributed this to the neuronal degeneration. On the other hand, Wallig *et al*., (2018)[43] stated that the cytoplasmic acidophilia is one of the hallmark features of toxicant-induced neuronal necrosis and referred these neurons as red necrotic ones.

Concerning the vacuolated cytoplasm of some pyramidal cells, this could be attributed to AlCl3-induced lipid peroxidation of cell and organelles membranes[44]. Additionally cell vacuolations occur upon water influx along with sodium ions due to failure of sodium-potassium pumps[45]. Some pyramidal cells showed corkscrew dendrites. This could be attributed to the helical arrangement of neurofilaments within the dendrites affected by the oxidative stress[46].

Some neuroglial cells were fused together with an apparent microgliosis. Similar findings were observed by Fahmy *et al*., (2020)[47]. This could be attributed to activation of the neuroglia after exposure to neurotoxic agents. The microglial cells accumulate and exhibit a great capacity to phagocytose dead neurons[48].

In addition, the neuropil appeared vacuolated. Nallagouni & Reddy, (2017)[49] referred this as spongiosis and attributed it to edema within the neuropil as a result of the increased permeability of the blood brain barrier (BBB). Some areas with focal hemorrhage were also noticed. This was in agreement with Abdelghany *et al*., (2019)[50]. AlCl3 can alter the permeability of BBB by disrupting the junctional complexes between the endothelial cells[51]. Additionally, the neuroglia which infiltrate the injured areas secrete matrixmetallo-proteinases (MMPs) which break the basal lamina and tight junction proteins[52].

At the ultrastructural level, the perinuclear cisternae of some cells were dilated. This may be due to cellular apoptosis[53] or lipid peroxidation of nuclear membranes[54]. Additionally, swollen mitochondria were observed. Oxidative stress can disturb the permeability of mitochondrial membrane to ions with subsequent water accumulation[55]. Moreover, oxidative stress can contribute to opening of mitochondrial permeability transition pore (mPTP) which leads to increase in membranes permeability[56]. Numerous lysosomes were observed in some cells. This could be attributed to the compensatory lysosomal biogenesis to enhance heterophagy and autophagy of the intracellular debris[57]. The myelin sheath illustrated splitting of its layers. Meknatkhah *et al*., 2019[58] reported that oxidative stress can cause myelin sheath decomposition due to disturbance in protein and lipid synthesis.

The Congo red stain revealed many Congo red positive pyramidal cells with amyloid granules in subgroup E1. This was in agreement with Nikmahzar *et al*., (2018)[59]. Upon reaction with Al ions, the cellular polypeptides undergo misfolding, denaturation and conformational alteration into β-amyloid which accumulates as intracellular amyloid granules. The proteasomes fail to degrade these proteins with amyloid accumulation, which is one of the pathognomonic features of AD. Deposition of amyloid can result in neuroinflammation, degeneration and neuronal loss[60]. Moreover, AlCl3 has anti-amyloidolytic action by preventing degradation of the amyloid peptides[61].

The present study revealed intracellular neurofibrillary tangles in the pyramidal cells in subgroup E1. The neuronal cell body and processes contain a microtubule associated tau protein. AlCl3 can induce hyperphosphorylation of tau by activating glycogen synthase kinase-3β (GSK-3β) enzyme, with misfolding into neurofibrillary tangles, the second pathognomonic hallmark feature of AD[62,63].

The current study demonstrated that AlCl3 administration attenuated the synaptic transmission as indicated by a statistically highly significant decrease in the expression of synaptophysin. This was in consistent with Yang *et al*., (2018)[64]. Synaptophysin is the most abundant presynaptic glycoprotein in membranes of neurotransmitter-containing vesicles with an important role in regulation of neurotransmitter release[65].

Neurotransmitter release from synaptic vesicles requires a coordinated binding of vesicle soluble N-ethylmaleimide-sensitive factor [NSF] attachment protein receptor (vSNARE)-vesicle associated membrane protein 2 (VAMP2) on the synaptic vesicle and the cognate target soluble NSF attachment protein receptor (tSNARE) on the target presynaptic membrane. Synaptophysin forms a complex with VAMP2. This complex is necessary to recruit VAMP2 to synaptic contacts. β-amyloid competes with VAMP2 for binding to synaptophysin with disruption of synaptophysin/VAMP2 complex and downregulates synaptophysin expression with ultimate synaptic dysfunction[66,67].

In the current study, the media-treated subgroup revealed similar results as the AlCl3-treated subgroup. This indicates that the media injection was not able to ameliorate the structural changes that were induced by AlCl3.

It was observed that BM-MSCs partially improved the structural changes of in the present work. CA1 area showed proper arrangement of layers. Most of the pyramidal and neuroglial cells were more or less normal. Similar findings were observed by Tang *et al*., (2017)[68] during the study of neuronal repair by MSCs after ischemic injury.

These observations may be attributed to the paracrine functions of MSCs that are related to secretion of several trophic factors including cytokines and chemokines into the surrounding area. It has been reported that MSCs possess anti-apoptotic, anti-oxidant, anti-inflammatory, immunomodulatory and angiogenic properties. Moreover, MSCs can introduce neurotrophic factors that maintain

neuronal survival[69,70].

The anti-apoptotic effect of MSCs is associated with a decrease in the expression of pro-apoptotic molecules and an increase in the anti-apoptotic ones[71]. This may occur via stimulation of cell survival signaling pathways, deactivation of cell death signals as caspase-3 and release of extracellular vesicles that increase blood flow to the injured area[72]. As regards the anti-oxidant effect, MSCs can increase the expression of anti-oxidant enzymes as superoxide dismutase and catalase. Furthermore, MSCs can suppress the lipid peroxidation associated with oxidative stress[73]. The anti-inflammatory and immunomodulatory effects of MSCs have been attributed to their ability to secrete anti-inflammatory factors including tumor necrosis factor-β1 (TNF-β1) and neurotrophin-3 (NT-3). The MSCs can inhibit secretion of pro-inflammatory cytokines as interferon-γ (IFN-γ) and tumor necrosis factor-α (TNF-α)[74,75].

On the other hand, previous researchers suggested that the therapeutic effect of MSCs is mainly related to their differentiation capacity. They reported that MSCs can cross the BBB through paracellular pathway as they can affect the tight junctions of the endothelial cells leading to their temporary abolishment with subsequent homing into the injured brain tissue. Later on, the MSCs either differentiate into neural cell lineages including neurons and neuroglia, or release chemokines that enhance proliferation, migration and differentiation of the endogenous native neural stem cells[76,77].

Ultrastructural examination of the blood capillaries in the BM-MSCs-treated subgroup revealed apparently normal basement membranes. After settlement in the injured tissue, the MSCs attenuate secretion of MMPs from the neuroglial cells. The tight junction and basal lamina proteins are restored[52]. The myelin sheath appeared more or less normal. The MSCs can produce factors which induce oligodendrogenesis by reducing the anti-oligodendrogenic determinant inhibitor of differentiation-2 (Id2) and increasing the pro-oligodendrogenic oligodendrocytes transcription factor-2 (Olig2) in the neural progenitor cells. Therefore, generating more functioning oligodendrocytes in the injured area with repair of the degenerated myelin sheath[78,79].

A few number of Congo red positive pyramidal cells in BM-MSCs-treated subgroup was observed. The MSCs can reduce β-amyloid generation and enhance β-amyloid uptake by the local microglial cells by phagocytosis or receptor mediated endocytosis[80]. Furthermore, the MSCs have an anti-amyloidogenic potential[81]. The current study revealed that BM-MSCs reduced the neurofibrillary tangles. The MSCs could reduce tau hyperphosphorylation by inactivating GSK-3β enzyme with reduction in accumulation of neurofibrillary tangles[60].

Immunohistochemically, there was a non-significant difference in the mean color intensity of synaptophysin in BM-MSCs-treated subgroup as compared with control group. The MSCs can restore synaptogenesis and enhance expression of synaptic proteins including synaptophysin[81,82].

The present work revealed a minimal improvement of the structural changes that were induced by AlCl3 in the recovery subgroup. This could be attributed to the limited regenerative capacity of CNS due to the inhibitory environment of the injured tissue[83]. The activated neuroglial cells migrate to site of injury, where they form a tight interpenetrating network known as reactive glial scar to buffer the cytotoxic molecules and isolate the site of injury. However, the neuroglial cells that persist at site of injury produce inhibitory factors including chondroitin sulfate proteoglycans and tenascins that severely limit neuroregeneration. In addition, the injured neurons of adult CNS are only capable of minimal regeneration[84,85].

CONCLUSION

BM-MSCs injection could ameliorate the AD-like pathology which was induced by AlCl3 in CA1 area of the hippocampus of adult male albino rat. Further clinical studies are needed to investigate the possibility of applying BM-MSCs as a line of human AD therapy.

ACKNOWLEDGEMENT

CONFLICT OF INTERESTS

There are no conflicts of interest.

REFERENCES

1. Spires-Jones TL and Ritchie CW: A brain boost to fight Alzheimer's disease. Science. (2018) 361(6406): 975-976.

2. Krajcovicova L, Mikl M, Marecek R and Rektorova I: Disturbed default mode network connectivity patterns in Alzheimer's disease associated with visual processing. Journal of Alzheimer's Disease: JAD. (2014) 41(4): 1229-1238.

3. Waite LM: Treatment for Alzheimer's disease: has anything changed? Australian Prescriber. (2015) 38(2): 60-63.

4. Alzheimer's Association: 2016 Alzheimer's disease facts and figures. Alzheimer's & Dementia. (2016) 12(4): 459-509.

5. Kocahan S and Dogan Z: Mechanisms of Alzheimer's disease pathogenesis and prevention: The brain, neural pathology, N-methyl-D-aspartate receptors, tau protein and other risk factors. Clinical Psychopharmacology and Neuroscience. (2017) 15(1): 1-8.

6. Chu LW: Alzheimer's disease: early diagnosis and treatment. Hong Kong Medical Journal. (2012) 18(3): 228-237.

7. Mendiola-Precoma J, Berumen LC, Padilla K and Garcia-Alcocer G: Therapies for prevention and treatment of Alzheimer's disease. BioMed Research International. (2016) 2016: 2589276.

8. Nelson L and Tabet N: Slowing the progression of Alzheimer's disease; what works? Ageing Research Reviews. (2015) 23(Pt B): 193-209.

9. Moraes MU and Gaudet TJ: Immunotherapeutic and pharmacological approaches for the treatment of Alzheimer's disease. Bioscience Horizons: The International Journal of Student Research. (2018) 11:hzy001 (1-7).

10. Ulusoy HB, Sonmez MF, Kilic E, Caliskan K, Karaca B, Kara M, Ercal O, Gunduz Y, Karabulut D, Bitiktas S, Tan B, Kavraal S, Inal A and Suer C: Intraperitoneal administration of low dose aluminium in the rat: How good is it to produce a model for Alzheimer disease. Archives Italiennes de Biologie. (2015) 153(4): 266-278.

11. Ge M, Zhang Y, Hao Q, Zhao Y and Dong B: Effects of mesenchymal stem cells transplantation on cognitive deficits in animal models of Alzheimer's disease: A systematic review and meta-analysis. Brain and Behavior. (2018) 8(7): e00982.

12. Fu Y, Karbaat L, Wu L, Leijten J, Both SK and Karperien M: Trophic effects of mesenchymal stem cells in tissue regeneration. Tissue Engineering Part B Reviews. (2017) 23(6): 515-528.

13. Padurariu M, Ciobica A, Mavroudis I, Fotiou D and Baloyannis S: Hippocampal neuronal loss in the CA1 and CA3 areas of Alzheimer's disease patients. Psychiatria Danubina. (2012) 24(2): 152-8.

14. Ghoneim FM, Khalaf HA, Elsamanoudy AZ, Abo El-Khair SM, Helaly AM, Mahmoud el-HM and Elshafey SH: Protective effect of chronic caffeine intake on gene expression of brain derived neurotrophic factor signaling and the immunoreactivity of glial fibrillary acidic protein and Ki-67 in Alzheimer's disease. International Journal of Clinical and Experimental Pathology. (2015) 8(7): 7710-7728.

15. Piccinini F, Tesei A, Arienti C and Bevilacqua A: Cell counting and viability assessment of 2D and 3D cell cultures: Expected reliability of the trypan blue assay. Biological Procedures Online. (2017) 19:8.

16. Yusop N, Battersby P, Alraies A, Sloan AJ, Moseley R and Waddington RJ: Isolation and characterisation of mesenchymal stem cells from rat bone marrow and the endosteal niche: A comparative study. Stem Cells International. (2018) 2018: 6869128.

17. Salem AM, Ahmed HH, Atta HM, Ghazy MA and Aglan HA: Potential of bone marrow mesenchymal stem cells in management of Alzheimer's disease in female rats. Cell Biology International. (2014) 38(12): 1367-1383.

18. Ahmed HH, Salem AM, Sabry GM, Husein AA, Soheir E and Kotob SE: New insights in the horizon for the treatment of Alzheimer's disease: A proposal based on experimental study. Der Pharmacia Lettre. (2015) 7(2): 165-182.

19. Kushawaha S, Malpani A, Aswar UM, Bodhankar SL, Malpani A and Shivakumar S: Effect of different anesthetic agents on cardiovascular parameters in male wistar rats. Research Journal of Pharmaceutical, Biological and Chemical Sciences. (2011) 2(2): 685-690.

20. Hajipour S, Sarkaki A, Farbood Y, Eidi A, Mortazavi P and Valizadeh Z: Effect of gallic acid on dementia type of Alzheimer disease in rats: Electrophysiological and histological studies. Basic and Clinical Neuroscience. (2016) 7(2): 97-106.

21. Bancroft JD and Layton C: The Hematoxylins and Eosin. In: Suvarna SK, Layton C and Bancroft JD. Bancroft's Theory and Practice of Histological Techniques. 8th ed., Elsevier, Philadelphia. (2019) pp: 126.

22. Jahanshahi M, Nikmahzar E and Sayyahi A: Vitamin E therapy prevents the accumulation of congophilic amyloid plaques and neurofibrillary tangles in the hippocampus in a rat model of Alzheimer's disease. Iranian Journal of Basic Medical Sciences. (2020) 23(1): 86-92.

23. Xiaoguang W, Jianjun C, Qinying C, Hui Z, Lukun Y and Yazhen S: Establishment of a valuable mimic of Alzheimer's disease in rat animal model by intracerebroventricular injection of composited amyloid beta protein. Journal of Visualized Experiments: JoVE. (2018) 137: 56157.

24. Wadhwa M, Sahu S, Kumari P, Kauser H, Ray K and Panjwani U: Caffeine and modafinil given during 48 h sleep deprivation modulate object recognition memory and synaptic proteins in the hippocampus of the rat. Behavioural Brain Research. (2015) 294:95-101.

25. Bozzola JJ and Russell LD: Electron Microscopy: Principles and Techniques for Biologists. 2nd ed., Jones and Bartlett Publishers, Boston, Toronto, London, Singapore. (1999) pp: 17.

26. Kuo J.: Electron Microscopy: Methods and Protocols. 2nd ed., Humana Press Inc. Totowa, New Jersey. (2007) pp: 19.

27. Mahmoud FY, Abd El-Hakim AH, Amer AS and Fidal MW: Effect of exposure to cadmium on the hippocampus in adult albino rat and the possible role of L-carnitine. Journal of Current Medical Research and Practice. (2019) 4(3): 240-250.

28. Fang Y, Gao T, Zhang B and Pu J: Recent advances: Decoding Alzheimer's disease with stem cells. Frontiers in Aging Neuroscience. (2018) 10: 77.

29. Chiroma SM, Hidayat Baharuldin MT, Mat Taib CN, Amom Z, Jagadeesan S, Adenan MI and Mohd Moklas MA: Protective effect of Centella asiatica against D-galactose and aluminium chloride induced rats: Behavioral and ultrastructural approaches. Biomedicine & Pharmacotherapy. (2019) 109: 853-864.

30. Auti ST and Kulkarni YA: Neuroprotective effect of cardamom oil against aluminum induced neurotoxicity in rats. Frontiers in Neurology. (2019) 10:399.

31. Al-Otaibi SS, Arafah MM, Sharma B, Alhomida AS and Siddiqi NJ: Synergistic effect of quercetin and α-lipoic acid on aluminium chloride induced neurotoxicity in rats. Journal of Toxicology. (2018) 2018: 2817036.

32. Saad HM, Hassieb MM, Oda SS, Tohamy HG and Khafaga AF: Histopathologic study on the toxic effect of aluminium chloride on the heart, liver and kidneys of rabbits. Alexandria Journal of Veterinary Sciences. (2018) 56(1): 102-109.

33. Singh A, Kukreti R, Saso L and Kukreti S: Oxidative stress: A key modulator in neurodegenerative diseases. Molecules. (2019) 24(8): 1583.

34. Zaher MF, Bendary MA, Abd El-Aziz GS and Ali AS: Potential protective role of thymoquinone on experimentally-induced Alzheimer rats. Journal of Pharmaceutical Research International. (2019) 31(6): 1-18.

35. Kaufmann W, Bolon B, Bradley A, Butt M, Czasch S, Garman RH, George C, Gröters S, Krinke G, Little P, McKay J, Narama I, Rao D, Shibutani M and Sills R: Proliferative and nonproliferative lesions of the rat and mouse central and peripheral nervous systems. Toxicologic Pathology. (2012) 40(4): 87S-157S.

36. Kaler S, Dhar P, Bhattacharya A and Mehra RD: Preliminary morphological and immunohistochemical changes in rat hippocampus following postnatal exposure to sodium arsenite. Toxicology International. (2013) 20(2): 160-169.

37. Kumar V, Abbas AK and Aster JC: Robbins Basic Pathology. 10th ed., Elsevier, Philadelphia. (2018): pp: 35.

38. Murugan MS and Bhargavan R: Neuroprotective effect of Bacopa monnieri against aluminum chloride-induced oxidative stress and apoptosis in the hippocampus of Wistar rats. Drug Invention Today. (2020) 14(3): 164-169.

39. Telegina DV, Suvorov GK, Kozhevnikova OS and Kolosova NG: Mechanisms of neuronal death in the cerebral cortex during aging and development of Alzheimer's disease-like pathology in rats. International Journal of Molecular Sciences. (2019) 20(22): 5632.

40. Battistelli M and Falcieri E: Apoptotic bodies: Particular extracellular vesicles involved in intercellular communication. Biology (Basel). (2020) 9(1): 21.

41. Bharathi MD and Thenmozhi AJ: Attenuation of aluminum-induced neurotoxicity by tannoid principles of emblica officinalis in wistar rats. International Journal of Nutrition, Pharmacology, Neurological Diseases. (2018) 8(2): 35-40.

42. Haider S, Liaquat L, Ahmad S, Batool Z, Siddiqui RA, Tabassum S, Shahzad S, Rafiq S and Naz N: Naringenin protects AlCl3/D-galactose induced neurotoxicity in rat model of AD via attenuation of acetylcholinesterase levels and inhibition of oxidative stress. PLoS One. (2020) 15(1): e0227631.

43. Wallig MA, Haschek WM, Rousseaux CG, Bolon B and Mahler BW: Fundamentals of Toxicologic Pathology. 3rd ed., Elsevier. London, San Diego, Cambridge. (2018) pp: 649.

44. Baranauskaite J, Sadauskiene I, Liekis A, Kasauskas A, Lazauskas R, Zlabiene U, Masteikova R, Kopustinskiene DM and Bernatoniene J: Natural compounds rosmarinic acid and carvacrol counteract aluminium-induced oxidative stress. Molecules. (2020) 25(8): 1807.

45. Miller MA and Zachary JF: Mechanisms and Morphology of Cellular Injury, Adaptation, and Death. In: Zachary JF. Pathologic Basis of Veterinary Disease. 6th ed., Elsevier. Philadelphia. (2017) pp: 11.

46. Acharya NK, Levin EC, Clifford PM, Han M, Tourtellotte R, Chamberlain D, Pollaro M, Coretti NJ, Kosciuk MC, Nagele EP, Demarshall C, Freeman T, Shi Y, Guan C, Macphee CH, Wilensky RL and Nagele RG: Diabetes and hypercholesterolemia increase blood-brain barrier permeability and brain amyloid deposition: beneficial effects of the LpPLA2 inhibitor darapladib. Journal of Alzheimer's disease: JAD. (2013) 35(1): 179-198.

47. Fahmy HM, Aly EM, Mohamed FF, Noor NA and Elsayed AA: Neurotoxicity of green-synthesized magnetic iron oxide nanoparticles in different brain areas of wistar rats. Neurotoxicology. (2020) 77: 80-93.

48. Wu T and Tang M: The inflammatory response to silver and titanium dioxide nanoparticles in the central nervous system. Nanomedicine. (2018) 13(2): 233-249.

49. Nallagouni CS and Reddy KP: Aluminum and fluoride impacts cortex and hippocampus structure in rats: Protective role of resveratrol. International Journal of Applied Biology and Pharmaceutical Technology. (2017) 8(1): 89-97.

50. Abdelghany AK, Khalil F, Azeem NMA, EL-Nahass E, EL-Kashlan AM and Emeash HH: Ginseng and moringa olifera ameliorated cognitive impairments induced by aluminium chloride in albino rat. Advances in Animal and Veterinary Sciences. (2019) 7(7): 557-565.

51. Bekhedda H, Menadi N, Demmouche A, Ghani A and Mai H: Histological study of the effects of aluminum chloride exposure on the brain of wistar rats female. Journal of Drug Delivery & Therapeutics. (2020) 10(3-S): 37-42.

52. Cheng Z, Wang L, Qu M, Liang H, Li W, Li Y, Deng L, Zhang Z and Yang GY: Mesenchymal stem cells attenuate blood-brain barrier leakage after cerebral ischemia in mice. Journal of Neuroinflammation. (2018) 15(1): 135.

53. Abdel-Aal RA, Farghaly HS and Zakaria AZ: Lamotrigine enhances the neuroprotective effects of memantine on aluminum chloride-induced behavioral changes in rats. Journal of Current Medical Research and Practice. (2018) 3(3): 171-179.

54. El Gharabawy GS, Abd Allah EE, Amr IM and Elmitwalli M: Histological and immunohistochemical study of the effect of cyclophosphamide on testis of male adult albino rats and the possible protective role of vitamin E. The Egyptian Journal of Hospital Medicine. (2019) 77(6): 5930-5946.

55. Barkhade T, Mahapatra SK and Banerjee I: Study of mitochondrial swelling, membrane fluidity and ROS production induced by nano-TiO2 and prevented by Fe incorporation. Toxicology Research. (2019) 8(5): 711-722.

56. Frati A, Cerretani D, Fiaschi AI, Frati P, Gatto V, La Russa R, Pesce A, Pinchi E, Santurro A, Fraschetti F and Fineschi V: Diffuse axonal injury and oxidative stress: A comprehensive review. International Journal of Molecular Sciences. (2017) 18(12): 2600.

57. Pi H, Li M, Tian L, Yang Z, Yu Z and Zhou Z: Enhancing lysosomal biogenesis and autophagic flux by activating the transcription factor EB protects against cadmium-induced neurotoxicity. Scientific Reports. (2017) 7: 43466.

58. Meknatkhah S, Sharif Dashti P, Mousavi MS, Zeynali A, Ahmadian S, Karima S, Saboury AA and Riaziet GH: Psychological stress effects on myelin degradation in the cuprizone-induced model of demyelination. Neuropathology: Official Journal of The Japanese Society of Neuropathology. (2019) 39(1): 14-21.

59. Nikmahzar E, Jahanshahi M and Babakordi F: Ginkgo biloba extract decreases scopolamine-induced congophilic amyloid plaques accumulation in male rat's brain. Jundishapur Journal of Natural Pharmaceutical Products. (2018) 13(4): e69143.

60. Zhao Y, Chen X, Wu Y, Wang Y, Li Y and Xiang C: Transplantation of human menstrual blood-derived mesenchymal stem cells alleviates Alzheimer's disease-like pathology in APP/PS1 transgenic mice. Frontiers in Molecular Neuroscience. (2018) 11: 140.

61. Igbokwe IO, Igwenagu E and Igbokwe NA: Aluminium toxicosis: a review of toxic actions and effects. Interdisciplinary Toxicology. (2019) 12(2): 45-70.

62. Kumar SEP, Bairy KL, Nayak V, Reddy SK, Kiran A and Ballal A: Amelioration of aluminium chloride (AlCl3) induced neurotoxicity by combination of rivastigmine and memantine with artesunate in albino wistar rats. Biomedical & Pharmacology Journal. (2019) 12(2): 703-711.

63. Uddin MS, Kabir MT, Niaz K, Jeandet P, Clément C, Mathew B, Rauf A, Rengasamy KRR, Sobarzo-Sánchez E, Ashraf GM and Aleya L: Molecular insight into the therapeutic promise of flavonoids against Alzheimer's disease. Molecules. (2020) 25(6): 1267.

64. Yang X, Yao C, Tian T, Li X, Yan H, Wu J, Li H, Pei L, Liu D, Tian Q, Zhu LQ and Lu Y: A novel mechanism of memory loss in Alzheimer's disease mice via the degeneration of entorhinal-CA1 synapses. Molecular Psychiatry. (2018) 23(2): 199-210.

65. Alghamdi BS and AboTaleb HA: Melatonin improves memory defects in a mouse model of multiple sclerosis by up-regulating cAMP-response element-binding protein and synapse-associated proteins in the prefrontal cortex. Journal of Integrative Neuroscience. (2020) 19(2): 229-237.

66. Russell CL, Semerdjieva S, Empson RM, Austen BM, Beesley PW and Alifragis P.: Amyloid-β acts as a regulator of neurotransmitter release disrupting the interaction between synaptophysin and VAMP2. PLoS One. (2012) 7(8): e43201.

67. Adams DJ, Shen C, Levenga J, Basta T, Eisenberg SP, Mapes J, Hampton L, Grounds K, Hoeffer CA and Stowell MHB: Synaptophysin is a β-amyloid target that regulates synaptic plasticity and seizure susceptibility in an Alzheimer's model. bioRxiv: The Preprint Server for Biology (bioRxiv). (2017) doi: https://doi.org/10.1101/129551.

68. Tang X, Chen F, Lin Q, You Y, Ke J and Zhao S: Bone marrow mesenchymal stem cells repair the hippocampal neurons and increase the expression of IGF-1 after cardiac arrest in rats. Experimental and Therapeutic Medicine. (2017) 14(5): 4312-4320.

69. Barzegar M, Kaur G, Gavins FNE, Wang Y, Boyer CJ and Alexander JS: Potential therapeutic roles of stem cells in ischemia-reperfusion injury. Stem Cell Research. (2019) 37: 101421.

70. Mancuso P, Raman S, Glynn A, Barry F and Murphy JM: Mesenchymal stem cell therapy for osteoarthritis: The critical role of the cell secretome. Frontiers in Bioengineering and Biotechnology. (2019) 7: 9.

71. Mukhamedshina YO, Gracheva OA, Mukhutdinova DM, Chelyshev YA and Rizvanov AA: Mesenchymal stem cells and the neuronal microenvironment in the area of spinal cord injury. Neural Regeneration Research. (2019) 14(2): 227-237.

72. Zhang Y, Yu S, Tuazon JP, Lee JY, Corey S, Kvederis L, Kingsbury C, Kaneko Y and Borlongan CV: Neuroprotective effects of human bone marrow mesenchymal stem cells against cerebral ischemia are mediated in part by an anti-apoptotic mechanism. Neural Regeneration Research. (2019) 14(4): 597-604.

73. Angeloni C, Gatti M, Prata C, Hrelia S and Maraldi T: Role of mesenchymal stem cells in counteracting oxidative stress-related neurodegeneration. International Journal of Molecular Sciences. (2020) 21(9): 3299.

74. Legaki E, Roubelakis MG, Theodoropoulos GE, Lazaris A, Kollia A, Karamanolis G, Marinos E and Gazouli M: Therapeutic potential of secreted molecules derived from human amniotic fluid mesenchymal stem/stroma cells in a mice model of colitis. Stem Cell Reviews and Reports. (2016) 12(5): 604-612.

75. Pokrovskaya LA, Zubareva EV, Nadezhdin SV, Lysenko AS and Litovkina TL: Biological activity of mesenchymal stem cells secretome as a basis for cell-free therapeutic approach. Research Results in Pharmacology. (2020) 6(1): 57-68.

76. Hasan A, Deeb G, Rahal R, Atwi K, Mondello S, Marei HE, Gali A and Sleiman E: Mesenchymal stem cells in the treatment of traumatic brain injury. Frontiers in Neurology. (2017) 8: 28.

77. Dabrowska S, Andrzejewska A, Lukomska B and Janowski M: Neuroinflammation as a target for treatment of stroke using mesenchymal stem cells and extracellular vesicles. Journal of Neuroinflammation. (2019) 16(1): 178.

78. Steffenhagen C, Dechant FX, Oberbauer E, Furtner T, Weidner N, Kury P, Aigner L and Rivera FJ: Mesenchymal stem cells prime proliferating adult neural progenitors toward an oligodendrocyte fate. Stem Cells and Development. (2012) 21(11): 1838-1851.

79. Mukhamedshina YO, Gracheva OA, Mukhutdinova DM, Chelyshev YA and Rizvanov AA: Mesenchymal stem cells and the neuronal microenvironment in the area of spinal cord injury. Neural Regeneration Research. (2019) 14(2): 227-237.

80. Yokokawa K, Iwahara N, Hisahara S, Emoto MC, Saito T, Suzuki H, Manabe T, Matsumura A, Matsushita T, Suzuki S, Kawamata J, Sato-Akaba H, Fujii HG and Shimohama S: Transplantation of mesenchymal stem cells improves amyloid-β pathology by modifying microglial function and suppressing oxidative stress. Journal of Alzheimer's Disease: JAD. (2019) 72(3): 867-884.

81. Fouad GI: Stem cells as a promising therapeutic approach for Alzheimer's disease: a review. Bulletin of the National Research Centre. (2019) 43(1): 52.

82. Ding SL: Comparative anatomy of the prosubiculum, subiculum, presubiculum, postsubiculum, and parasubiculum in human, monkey, and rodent. The Journal of Comparative Neurology. (2013) 521(18): 4145-4162.

83. Quraishe S, Forbes LH and Andrews MR: The extracellular environment of the CNS: Influence on plasticity, sprouting, and axonal regeneration after spinal cord injury. Neural plasticity. (2018) 2018: 2952386.

84. Filous AR and Schwab JM: Determinants of axon growth, plasticity, and regeneration in the context of spinal cord injury. The American Journal of Pathology. (2018) 188(1): 53-62.

85. Fawcett JW: The struggle to make CNS axons regenerate: Why has it been so difficult? Neurochemical Research. (2020) 45(1): 144-158.

الملخص العربى

تأثير الخلايا الجذعية الوسيطة المشتقة من نخاع العظم على منطقة قرن آمون (١) في الحصين في مرض الزهايمر المستحدث بكلوريد الألومنيوم في ذكر الجرذ الأبيض البالغ: دراسة هستولوجية وهستوكيميائية مناعية

إيمان محمد البلتاجي، هبة حسن القليني، خالد أحمد مصطفى، جيهان محمد سليمان وعبد المنعم فريد زمزم

قسم الهستولوجيا وبيولوجيا الخلية، كلية الطب، جامعة طنطا، مصر

المقدمة: يعتبر مرض الزهايمر هو السبب الأكثر شيوعًا للخرف بين كبار السن. ويعد الألومنيوم معدن سام حيث يؤثر بشكل أساسى على قرن آمون، ويعتبر العلاج بالخلايا الجذعية الوسيطة المشتقة من نخاع العظم استراتيجية حديثة لعلاج العديد من الأمراض متضمنة الأمراض العصبية.

الهدف من العمل: دراسة تأثير الخلايا الجذعية الوسيطة المشتقة من نخاع العظم على منطقة قرن آمون (١) فى مرض الزهايمر المستحدث تجريبياً في ذكر الجرذ الأبيض البالغ.

المواد والطرق: تم تقسيم ٣٥ من ذكور الجرذان البيضاء البالغة إلى مجموعتين رئيسيتين؛ المجموعة الضابطة والمجموعة التجريبية والتى تم تقسيمها إلى أربع مجموعات فرعية (المجموعة الفرعية التجريبية ١، ٢، ٣ و٤) حيث تناول جميع جرذان المجموعة التجريبية ١٧ مجم/كجم من كلوريد الألومنيوم عن طريق الفم مرة واحدة يومياً لمدة أربعة أسابيع، وقد تم حقن كل جرذ من المجموعة الفرعية التجريبية الثانية والثالثة بـ ١ مل من الوسط المستخدم لتعليق الخلايا الجذعية الوسيطة المشتقة من نخاع العظم و بالخلايا الجذعية الوسيطة المشتقة من نخاع العظم ($10^6 \times 3$) بالترتيب داخل الوريد مرة واحدة وذلك بعد ٢٤ ساعة من آخر جرعة من كلوريد الألومنيوم. بينما كانت المجموعة الفرعية التجريبية الرابعة مجموعة النقاهة، ثم تم الحصول على عينات قرن آمون لإجراء دراسات هستولوجية ومورفومترية وتحليل إحصائي.

النتائج: أظهرت المجموعة الفرعية التجريبية الأولى والثانية تغيرات تركيبية مثل عدم ترتيب في طبقة الخلايا الهرمية والتى احتوت على أنوية داكنة الصبغة وفجوات فى السيتوبلازم. وقد أظهرت صبغة الكونغو الحمراء خلايا هرمية ذات تفاعل إيجابى مع الصبغة فى هذه المجموعات الفرعية، كما كشف الفحص المجهري الإلكتروني العديد من التغيرات التركيبية الدقيقة مثل انتفاخ فى الميتوكوندريا واتساع فى أكياس جولجي. وقد أظهر التحليل الإحصائى ارتفاعاً ذا دلالة إحصائية عالية فى التشابكات الليفية العصبية وانخفاضاً في التفاعل المناعي لسينابتوفيسين. وفى المجموعة الفرعية المعالجة بالخلايا الجذعية الوسيطة المشتقة من نخاع العظم تم حدوث تحسن ملحوظ فى هذه التغيرات، بينما أظهرت مجموعة النقاهة استمراراً لهذه التغيرات التركيبية.

الإستنتاج: يستنتج من هذه الدراسة أن حقن الخلايا الجذعية الوسيطة المشتقة من نخاع العظم لديه القدرة على تحسين التغيرات المرضية الشبيهة بمرض الزهايمر المستحدث بكلوريد الألومنيوم في منطقة قرن آمون (١) لذكور الجرذان البيضاء البالغة.